How Wettability Controls Nanoprinting

Juan Carlos Fernández-Toledano,[1,*] Bertrand Braeckeveldt,[1] Marco Marengo,[2] and Joël De Coninck[1]
[1]Laboratory of Surface and Interfacial Physics (LPSI), Department of Physics, University of Mons, Mons 7000, Belgium
[2]Advanced Engineering Centre, University of Brighton, Brighton BN2 4GJ, United Kingdom

(Received 3 June 2019; accepted 26 May 2020; published 5 June 2020)

Using large scale molecular dynamics simulations, we study in detail the impact of nanometer droplets of low viscosity on flat substrates versus the wettability of the solid plate. The comparison between the molecular dynamics simulations and different macroscopic models reveals that most of these models do not correspond to the simulation results at the nanoscale, in particular for the maximal contact diameter during the nanodroplet impact ($D_{\max}$). We have developed a new model for $D_{\max}$ that is in agreement with the simulation data and also takes into account the effects of the liquid-solid wettability. We also propose a new scaling for the time required to reach the maximal contact diameter $t_{\max}$ with respect to the impact velocity, which is also in agreement with the observations. With the new model for $D_{\max}$ plus the scaling found for $t_{\max}$, we present a master curve collapsing the evolution of the nanometer drop contact diameter during impact for different wettabilities and different impact velocities. We believe our results may help in designing better nanoprinters since they provide an estimation of the maximum impact velocities required to obtain a smooth and homogenous coverage of the surfaces without dry spots.

DOI: 10.1103/PhysRevLett.124.224503

More and more applications demand a detailed understanding of nanodroplets, applications such as 3D nanoprinting, nanomedicine, phase-change cooling using nanosprays, and microdeposition processes [1–3]. Remarkable achievements have been obtained rather recently by printing organic molecules at the nanoscale [4]. The interest of such technology is clear: it is flexible, inexpensive, fast, addressable, and scalable. Most of the practical applications are based on the idea that a nanodrop is used as a carrier of some biological elements or nanoparticles of one sort or another. It then remains to evaporate the carrier, the solvent of the nanodrop, to have access to a patterned surface with interesting functionalities. The idea is simple, and the technology is already mature enough to make it work [4]. Now, depending on the type of solvent, the shape of the nanodrop will vary not only with time but also with the impact speed of the nanodrop. This is where wetting and impact dynamics become critical. It is rather obvious that for small volumes the evaporation time for the solvent will be fast. If it is faster than the time required for the liquid to spread, we will end up with different structures leading to different properties. It is therefore mandatory to understand how wettability affects impact at such a small scale since wettability and evaporation are also intimately related [5].

Due to the huge number of applications involved, drop impact has been intensively studied in the past years. These studies have focused on, for example, the modeling of the influence of the drop size on the time evolution of the dynamic contact angle and contact radii [6], the transition between the bounce, stick, or splash of nanodroplets [7,8], the impact of nanodroplets on textured surfaces [9], the droplet impact over inclined substrates studied experimentally [10] or by using molecular dynamics (MD) techniques [11], and the drop impact over a moving substrate [12]. Given the strong deformation of the droplet during impact, especially for cases with relatively high impact velocities, the evaluation of the dynamic contact angle is not very accurate in comparison with the measurement of the contact diameter of the drop. Furthermore, different models have been proposed to characterize the maximum spreading diameter of a drop at macroscale [13–18]. Most of these models are either empirical or based on energy balance plus viscous dissipation but not all take into account the wetting properties between the liquid and the solid phases [14,16,18]. Moreover, these models have been compared with experiments at a macroscopic scale, but their validity at the nanometric scale, which is essential for many of the applications described above, is still unknown.

In this study, we use large scale MD simulations conducted using LAMMPS software [19] to analyze the impact of nanodroplets with a typical diameter of $D_0 = 20.3$ nm onto flat substrates. MD allows us to tune fundamental parameters like strength of interactions between atoms in order to explore the details of nanoprinting. By studying how the drops behave versus their equilibrium contact angles and the impact speeds, we will get a better understanding of impact for nanoprinting, potentially leading to interesting optimizations.

All the atoms have the same mass m_0 and they interact between each other via a pairwise Lennard–Jones (LJ) potential $V_{ij} = -4C_{\mathrm{AB}}k_BT[(\sigma/r)^{12} - (\sigma/r)^6]$ where r is the distance between atoms, σ is the effective atom diameter, k_B is the Boltzmann constant and $T = 33$ K is

the temperature. The values of $\sigma = 0.35$ nm and $m_0 = 12$ g/mol are selected to model carbon-like atoms. By tuning the value of C_{AB} (coupling between type "A" and type "B" atoms), we are able to change the strength of the interaction between the two types of atoms. We keep constant the value of the solid-solid and liquid-liquid coupling to 1.0 ($C_{SS} = C_{LL} = 1$), and we only tune the liquid-solid coupling ($C_{LS} \in [0.4, 0.8]$), which enables us to explore different wettabilities with equilibrium contact angles $\theta^0 \in [132°, 78°]$ and thus study in detail the importance of this parameter at the nanoscale. The liquid is made of 10 648 linear molecules of eight atoms each. Atoms inside a molecule are linked through a FENE potential $V_F = -0.5\kappa R_0^2 \ln[1 - (r/R_0)^2]$, where r is the distance between atoms, $\kappa = 12.25\epsilon/\sigma^2$, and $R_0 = 1.4\sigma$ is the maximum extension length. The solid substrate is modeled as 299 040 atoms distributed in a cubic lattice over a disk with a radius of 69.8 nm and three layers of atoms where the lattice parameter is equal to the location of the minima of the Lennard–Jones potential, i.e., $2^{1/6}\sigma \approx 0.39$ nm. The corresponding atoms are allowed to vibrate around an equilibrium position by introducing a harmonic potential that bonds the solid atoms to their initial positions. The corresponding harmonic potential is $V_h = 200\epsilon(r - r_0)^2$, where r_0 represents the equilibrium position of the solid atoms in the lattice. The cutoff of all the interactions is set to 2.5σ, and the time step between each interaction evaluation is fixed to 5 fs. For simplicity, we have not considered the presence of a surrounding fluid, which seems not to have a strong influence during the spreading process [7,20] although it can be critical for splashing [20].

Each simulation consists of two steps. In the first one, we equilibrate the system with the liquid atoms initially distributed in a square box far away from the influence of the substrate. During the equilibration, the temperature is kept constant by rescaling all the velocities. The equilibrium stage is achieved when the energy is constant versus time and the droplet shows a spherical cap shape of constant diameter $D_0 = (20.28 \pm 0.24)$ nm. After the equilibration step, the thermostat of the liquid is removed in order to enable thermal exchanges between the two phases, thus allowing the liquid to dissipate energy within the solid. The drop is also translated just above the substrate to reduce the distance to cross before impact. Finally, an initial impact velocity $V_{imp} \in [10\ 200]$ m/s in the direction perpendicular to the solid is set to the drop in order to initiate the impact. By using standard methods [21], we compute the liquid surface tension $\gamma_L = (2.85 \pm 0.56)$ mN/m, the viscosity $\eta_L = (0.284 \pm 0.004)$ mPa · s, and the liquid density $\rho_L = (386 \pm 5)$ kg/m^3. The model is thus rather simple. However, it has been used previously to study drop spreading [22] and liquid bridges [23] and been shown to reproduce macroscopic properties such as Laplace pressure and Young's law adequately. We compute the instantaneous contact diameter as $D(t) = 2r_c(t)$, where $r_c(t)$ is the radial

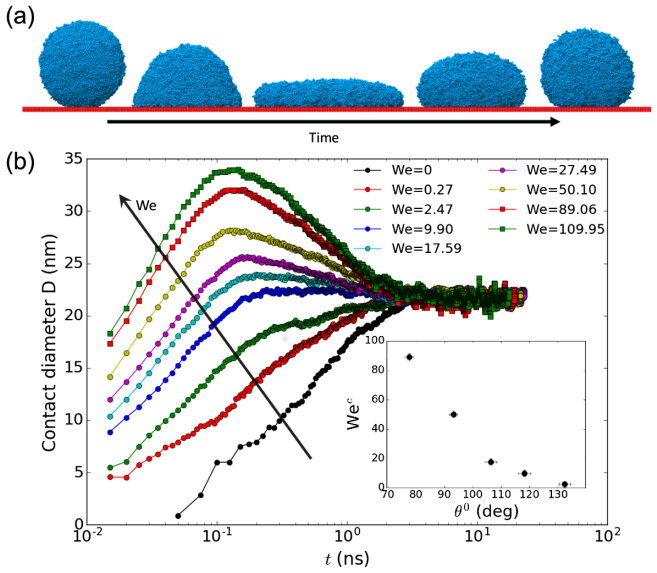

FIG. 1. (a) Snapshot of the simulations for $C_{LS} = 0.4$ ($\theta^0 = 132°$) and We = 109.9 at different times. (b) Droplet contact diameter versus time for various impact velocities for $C_{LS} = 0.6$ corresponding to the equilibrium contact angle $\theta^0 = 106°$.

distance with respect the mass center of the drop where the density of the liquid in contact with the plate drops at 50% of the value corresponding to the central part. Then, D_{max} corresponds just to the maximum value of $D(t)$ measured during the impact.

As a preliminary test, we study the increase of the liquid temperature ΔT with the impact velocity V_{imp}, which will introduce an increment of the kinetic energy on the drop that is converted to heat at impact, i.e., $\Delta T = V_{imp}^2/2c_v$, where c_v is the specific heat of the liquid. The specific heat can be measured from the energy fluctuations [24] in an independent simulation leading to the value of $c_v = (2533 \pm 380)$ J/kg · K. The increment of the temperature of the liquid can be measured in the simulations versus the impact velocities, and it has been observed that these values are independent of the considered wettability and are compatible with the expected theoretical value that corroborates the validity of the simulation methods.

First, we study the effect of the variation of the impact velocity V_{imp} on the dynamics of the droplet contact diameter. In order to compare our results with the different models presented in the literature, it is convenient to express V_{imp} as a dimensionless Weber number defined as $We = \rho_L D_0 V_{imp}^2/\gamma_L$ (the ratio of the liquid inertia and the surface tension), which is tuned between We = 0.27 ($V_{imp} = 10$ m/s) and We = 109.9 ($V_{imp} = 200$ m/s). Figure 1(a) shows different snapshots during the impact for $C_{LS} = 0.4$ ($\theta^0 = 132°$) and We = 109.9. In Fig. 1(b), we show the effect of the Weber number on the spreading dynamics for $C_{LS} = 0.6$ ($\theta^0 = 106°$). By increasing the

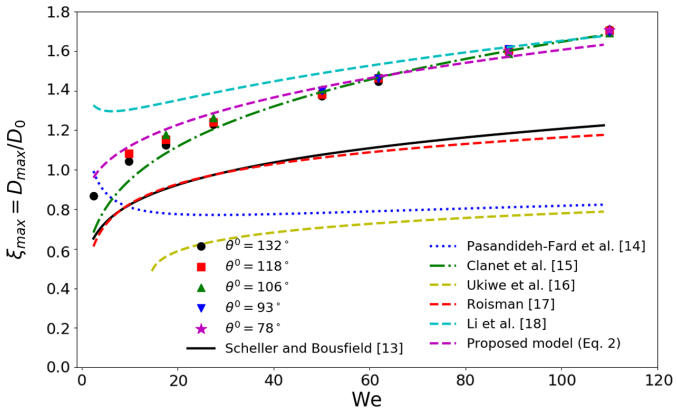

FIG. 2. $\xi_{\max} = D_{\max}/D_0$ versus the Weber number for all liquid-solid affinities studied and for $\mathrm{We} > \mathrm{We}^c$, i.e., when $D_{\max} > D_{\mathrm{eq}}$. The lines represent the different models proposed in the literature.

Weber number, the maximum contact diameter $D_{\max}$ rises within a considerable range (~34 nm) for a droplet of initial diameter of 20.3 nm, which is an expected result observed experimentally [14–16,25,26]. However, there are impact velocities for which the droplet never overcomes the equilibrium contact diameter D_{eq}. This can be seen in Fig. 1(b) for $\mathrm{We} < 30$. Let us here stress that this limit depends on the wettability of the plate. Therefore, there is a threshold in the Weber number We^c needed to reach a maximum spreading diameter larger than the equilibrium diameter, which is shown for the different equilibrium contact angles studied. It is clear that this critical impact in the inset of Fig. 1(b) for the different equilibrium contact angles studied. It is clear that this critical impact velocity We^c strongly depends on the wettability. However, as has been reported by other authors [15,25], when $\mathrm{We} > \mathrm{We}^c$, the time evolution of $D(t)$ until $D_{\max}$ is basically driven by inertia, the impact process is relatively insensitive to the surface wetting properties, and we get an increment of $D_{\max}$ when the solid-liquid affinity is decreased, as has been observed at low impact velocities ($\mathrm{We} < 30$). Let us here point out here that our results cannot be directly extrapolated to predict the properties of real superhydrophobic surfaces. Indeed, for such surfaces, superhydrophobicity is due to roughness that has not been introduced here. Therefore, the very low values of We^c for $\theta^0 > 120°$ do not necessarily imply that the impacts will be inertia driven in these substrates.

Figure 2 shows the values of $\xi_{\max} = D_{\max}/D_0$ for the different impact velocities (different We) and various liquid-solid equilibrium contact angles. $D_{\max}$ is here computed by a Gaussian fitting around the peak location on $D(t)$. For the lower impact velocity, there is an increment of $\xi_{\max}$ as the solid-liquid affinity is increased, but this difference disappears at higher impact velocities. However, once $D_{\max}$ is reached, we observe in the simulations that the wettability completely modifies the dewetting process until equilibrium, which can be very important in processes such as evaporating the solvent used to carry nanoparticles.

Many correlations and models have been proposed in the literature [13–15,17,27–30] to predict the time evolution of the maximum spreading factor $\xi_{\max}$. These correlations very rarely take into account the wettability effect, and they have been compared so far with experiments at the macroscale. In Fig. 2, we observe that the simulated $D_{\max}/D_0$ can be fitted with the power law $\xi_{\max} \propto \mathrm{We}^{1/4}$ introduced by Clanet *et al.* [15] for low viscous liquids based on the effective acceleration experienced by the drop during its impact. Clanet suggests that the initial kinetic energy due to the drop velocity is not only transformed to surface energy but also to internal kinetic energy. However, the value of this internal energy is not clear, and therefore, the complete description of $\xi_{\max}$ versus We without fitting parameters remains missing. As shown in Fig. 2, the semiempirical models derived from the energy balance [14,16,31] cannot describe properly the results for our low viscous liquid at the nanoscale. The origin of this discrepancy has certainly been located in the approximation used for the dissipation contribution, which considers that the velocity gradient only exists in the boundary layer adjacent to the liquid-solid interface [14]. Different approximations have been proposed [14,16,31] to describe the viscous dissipation in the impact of droplets at the macroscale. The validity of these approaches is uncertain at the nanoscale, however. Based on the analysis of the velocity distribution in MD simulations of water nanodroplet impacts, Li *et al.* [18] find that the velocity gradient not only exists in the boundary layer but is quite uniform in the droplet. With these considerations, they propose that the viscous dissipation for impact of nanodroplets can be written as $W = \pi\eta_L D_0^2 V_{\mathrm{imp}}(\xi_{\max}^2 - 2/3)/4$. However, as did Pasandideh–Fard *et al.* [14], they underestimate the liquid-vapor interface at the maximum spreading state in the energy balance equation, and the resulting prediction of $\xi_{\max}$ does not properly describe our simulation results as shown in Fig. 2.

Injecting the more precise approximation for the interfacial areas from Ref. [16] in the calculations, we obtain a new equation from the energy balance (see Supplemental Material [33] for details):

$$3(\mathrm{Ca} + 1 - \cos\theta^0)\xi_{\max}^3 - (\mathrm{We} + 12 + 2\mathrm{Ca})\xi_{\max} + 8 = 0, \tag{1}$$

where $\mathrm{Ca} = \eta_L V_{\mathrm{imp}}/\gamma_L$ is the capillary number associated with the impact velocity. Equation (1) has an analytical solution:

$$\xi_{\max} = 2\sqrt{-\frac{p}{3}}\cos\left[\frac{1}{3}\arccos\left(-\frac{q}{2}\sqrt{-\frac{27}{p^3}}\right)\right], \tag{2}$$

where $p = -(\mathrm{We} + 12 + 2\mathrm{Ca})/[3(\mathrm{Ca} + 1 - \cos\theta^0)]$ and $q = 8/[3(\mathrm{Ca} + 1 - \cos\theta^0)]$.

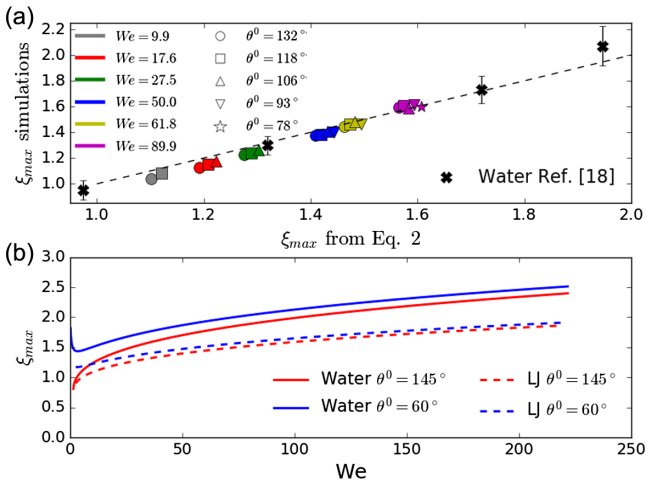

FIG. 3. (a) $\xi_{\max} = D_{\max}/D_0$ versus the Weber number for all liquid-solid affinities studied and the prediction from Eq. (2) for $\theta^0 = [132°, 78°]$. (b) Simulation results for impact of water nanodroplets from Ref. [18] and the model from Eq. (2) for water (continuous lines) and LJ (dashed lines) liquid with $\theta^0 = [145°, 60°]$.

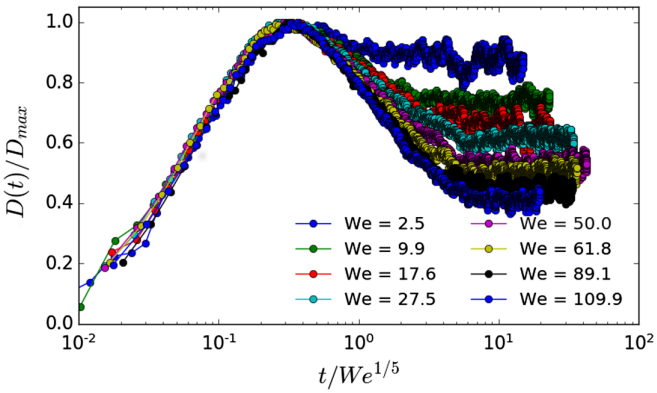

FIG. 4. Collapsing of $D/D_{\max}$ versus $t/\mathrm{We}^{-1/5}$ in a single curve for $\theta^0 = 132°$.

Figure 3(a) shows $D_{\max}$ measured from the simulation versus the prediction obtained from Eq. (2), where symbols and colors represent equilibrium contact angles and impact velocities, respectively. A good agreement between theory and simulation is observed. Also, our model predicts an increment of $D_{\max}$ when we increase the affinity between the liquid and the solid for low impact velocities, but the wettability effect becomes negligible for larger We. The proposed model is thus able to predict quite well not only the effect of the impact velocity but also the role of the wettability on $D_{\max}$.

The lack of experimental results for nanodroplet impacts impedes the comparison of Eq. (2) with real data. Nevertheless, we can validate the proposed model with the simulated results of water nanodroplets in platinum performed in Ref. [18], which can be also reproduced with the proposed model as shown in Fig. 3(a). Equation (2) also reveals that the role of the wettability depends on liquid properties. As an example, in Fig. 3(b) we show the $\xi_{\max}$ predicted by Eq. (2) for two liquids—our Lennard–Jones liquid and water—and two different substrate wettabilities. Interestingly, the effect of the wettability becomes more important for water due to its larger value of surface tension. As a result, Eq. (2) can be used in nanoprinting to predict the corresponding extension $D_{\max}$ from an initial droplet of diameter D_0 for any wettability θ_0 at any impact speed V_{imp}.

Let us now consider the time $t_{\max}$ at which the drop impacting the substrate reaches $D_{\max}$ whenever $D_{\max} > D_{\mathrm{eq}}$ corresponds to the case where $\mathrm{We} > \mathrm{We}^c$. For a precise detection of $t_{\max}$, we select a region around $D_{\max}$ and we fit a Gaussian distribution. We identify the central value of this Gaussian with $t_{\max}$. The representation of $t_{\max}$ can be modeled as a power law: $t_{\max}(\mathrm{ns}) = (0.319 \pm 0.016)\mathrm{We}^{-(0.196\pm0.014)}$ that basically corresponds to the scaling $t_{\max} \propto \mathrm{We}^{-1/5}$. This power law dependence of $t_{\max}$ has been observed experimentally at the macroscale with very similar exponents: for example, Antonini *et al.* [32] obtained $t_{\max} \propto \mathrm{We}^{-0.25}$ and Roux *et al.* [26] $t_{\max} \propto \mathrm{We}^{-0.32}$. With the resolution we have in the determination of $t_{\max}$, it is not possible to establish any influence of the wettability at the macroscale or nanoscale in the time required to achieve $D_{\max}$ that appears for $\mathrm{We} > \mathrm{We}^c$.

Once we have obtained $D_{\max}$ from Eq. (2) and with the power law $t_{\max} \propto \mathrm{We}^{-1/5}$, it is possible to transform the temporal evolution of the base diameter $D(t)$ into dimensionless units by dividing $D(t)$ and t by $D_{\max}$ and $\mathrm{We}^{-1/5}$, respectively. With this transformation, as can be seen in Fig. 4, all the data collapse into one universal curve before reaching the maximum spreading. Furthermore, this transformation works not only for different impact velocities but also for different substrate wettabilities, which we do not reproduce here for brevity, providing a good tool for nanoprinting. Therefore, it is possible to anticipate the temporal evolution of $D(t)$ at all impact velocities from a measurement of $D(t)$ at a single V_{imp}.

To conclude, in this study we have shown that MD is an interesting tool to analyze underlying mechanisms of drop impact for nanoprinting. MD allows us to probe molecular displacements and interactions during the whole process. We have shown that by increasing the impact velocity over a threshold value We^c, we increase the maximum spreading diameter of the droplet $D_{\max}$. We have also shown that $t_{\max}$, i.e., the time required to reach this maximum spreading, decreases as we increase the impact velocity. Moreover, we have studied the influence of the wettability over $D_{\max}$, $t_{\max}$, and We^c. We have shown that the threshold velocity We^c decreases as the contact angle increases. Also, we have found that $D_{\max}$ increases as the equilibrium contact angle between the liquid and the solid θ^0 is decreased for low impact velocities ($\mathrm{We}^c < \mathrm{We} < 30$) but it seems to be

independent of θ^0 when $We > We^c > 30$. However, t_{max} seems to be independent of the wettability for all equilibrium contact angles studied. We have proposed a new model to predict $\xi_{max} = D_{max}/D_0$ for nanodroplet impacts based on energy balance that successfully reproduces the simulation results and even the effect of changes in the wettability on D_{max} for low impact velocities. This model reveals the role of the substrate wettability, which could become important depending on liquid properties like surface tension and viscosity. Also, we have shown that $t_{max} \propto We^{-1/5}$, a scaling similar to the experimental observations. With the proposed models for D_{max} and t_{max}, we have seen that we can overlap in a master curve the evolution of the contact diameter $D(t)$ till D_{max} for all the impact velocities and all wettabilities used in this study. An interesting consequence of this work is that nanoprinting becomes predictable since we can estimate t_{max} as a function of the impact velocity and, from Eq. (2), we can predict D_{max}. However, experimental work on nanodroplet impacts is required to validate the approach proposed.

The authors thank the European Space Agency (ESA) and the Belgian Federal Science Policy Office (BELSPO) for their support in the framework of the PRODEX Programme. This research has also been partially funded by University of Mons (UMONS). Computational resources have been provided by the Consortium des Equipements de Calcul Intensif (CECI), funded by the Fonds de la Recherche Scientifique de Belgique (F. R. S.-FNRS) under Grant No. 2.5020.11.

*Corresponding author.
carlos.toledano@umons.ac.be

[1] A. Ishijima, K. Minamihata, S. Yamaguchi, S. Yamahira, R. Ichikawa, E. Kobayashi, M. Iijima, Y. Shibasaki, T. Azuma, T. Nagamune *et al.*, Sci. Rep. **7**, 44077 (2017).
[2] J. Ventrici de Souza, Y. Liu, S. Wang, P. Dörig, T. L. Kuhl, J. Frommer, and G.-Y. Liu, J. Phys. Chem. B **122**, 956 (2018).
[3] W. Wu, H. Bostanci, L. Chow, S. Ding, Y. Hong, M. Su, J. Kizito, L. Gschwender, and C. Snyder, Int. J. Heat Mass Transfer **54**, 2715 (2011).
[4] C. U. Hail, C. Höller, K. Matsuzaki, P. Rohner, J. Renger, V. Sandoghdar, D. Poulikakos, and H. Eghlidi, Nat. Commun. **10**, 1880 (2019).
[5] D. Brutin and V. Starovc, Chem. Soc. Rev. **47**, 558 (2018).
[6] N. Sedighi, S. Murad, and S. K. Aggarwal, Fluid Dyn. Res. **42**, 035501 (2010).
[7] J. Koplik and R. Zhang, Phys. Fluids **25**, 022003 (2013).
[8] A. Yarin, Annu. Rev. Fluid Mech. **38**, 159 (2006).
[9] R. Zhang, S. Farokhirad, T. Lee, and J. Koplik, Phys. Fluids **26**, 082003 (2014).
[10] J. Hao, J. Lu, L. Lee, Z. Wu, G. Hu, and J. M. Floryan, Phys. Rev. Lett. **122**, 054501 (2019).
[11] A. Delcorte and B. J. Garrison, Nucl. Instrum. Meth. B **303**, 179 (2013).
[12] H. Almohammadi and A. Amirfazli, Langmuir **33**, 5957 (2017).
[13] B. L. Scheller and D. W. Bousfield, AIChE J. **41**, 1357 (1995).
[14] M. Pasandideh-Fard, Y. M. Qiao, S. Chandra, and J. Mostaghimi, Phys. Fluids **8**, 650 (1996).
[15] C. Clanet, C. Béguin, D. Richard, and D. Quéré, J. Fluid Mech. **517**, 199 (2004).
[16] C. Ukiwe and D. Y. Kwok, Langmuir **21**, 666 (2005).
[17] I. V. Roisman, Phys. Fluids **21**, 052104 (2009).
[18] X.-H. Li, X.-X. Zhang, and M. Chen, Phys. Fluids **27**, 052007 (2015).
[19] S. Plimpton, J. Comput. Phys. **117**, 1 (1995).
[20] L. Xu, W. W. Zhang, and S. R. Nagel, Phys. Rev. Lett. **94**, 184505 (2005).
[21] M. P. Allen and D. J. Tildesley, *Computer Simulation of Liquids* (Clarendon Press, New York, NY, USA, 1989), ISBN 0-19-855645-4.
[22] E. Bertrand, T. D. Blake, and J. De Coninck, J. Phys. Condens. Matter **21**, 464124 (2009).
[23] J.-C. Fernandez-Toledano, T. D. Blake, P. Lambert, and J. De Coninck, Adv. Colloid Interface Sci. **245**, 102 (2017).
[24] H. B. Callen, *Thermodynamics and an Introduction to Thermostatistics* (Wiley, New York, 1985).
[25] R. Rioboo, M. Marengo, and C. Tropea, Exp. Fluids **33**, 112 (2002).
[26] D. C. D. Roux and J. J. Cooper-White, J. Colloid Interface Sci. **277**, 424 (2004).
[27] T. Mao, D. C. S. Kuhn, and H. Tran, AIChE J. **43**, 2169 (1997).
[28] H.-Y. Kim and J.-H. Chun, Phys. Fluids **13**, 643 (2001).
[29] J.-P. Delplanque and R. H. Rangel, J. Mater. Sci. **32**, 1519 (1997).
[30] P. Attané, F. Girard, and V. Morin, Phys. Fluids **19**, 012101 (2007).
[31] S. Chandra and C. T. Avedisian, Proc. R. Soc. Ser. A **432**, 13 (1991).
[32] C. Antonini, A. Amirfazli, and M. Marengo, Phys. Fluids **24**, 102104 (2012).
[33] See Supplemental Material at http://link.aps.org/supplemental/10.1103/PhysRevLett.124.224503 for detailed energy balance to obtain Eq. (1).